# Radiation Patterns Formed by Sapphire Capillary Needles with Different Shapes of Internal Channels

**Irina A. Shikunova***, **Dmitry O. Stryukov, Julia N. Zubareva, Anna S. Kucheryavenko, Vladimir N. Kurlov, and Irina N. Dolganova**
Osipyan Institute of Solid State Physics Russian Academy of Sciences, 2 Academician Osipyan str., Chernogolovka, Moscow District 142432, Russian Federation
*e-mail: sh_irina@issp.ac.ru

**Abstract.** Compact sapphire capillary needles for laser-assisted therapy connected to optical fibers by the means of internal channel closed from one side transmit laser radiation to the tissues with minimal loss of energy and simultaneously protect the fibers. The geometry of the internal capillary channel with the curved bottom is a key factor in the formation of the output beam's shape. Various curvatures of the bottom in combination with the different angle of conical needle's tip are studied in detail. When the tissue is covered in a liquid, we have observed forming the ring radiation pattern with a sharp axial peak without additional diaphragms or spatial light modulators. Coagulation of *ex vivo* liver tissue samples using continuous laser source with 1.06 μm wavelength, offered opportunity to obtain small coagulated spots without carbonization with the diameter of at least 0.8 mm and to enlarge them evenly by tuning the source output power. © 2024 Journal of Biomedical Photonics & Engineering.

**Keywords:** sapphire shaped crystals; fiber optic irradiators; laser therapy; interstitial laser irradiation; microfocusing.

Paper #9174 received 7 Oct 2024; revised manuscript received 18 Nov 2024; accepted for publication 18 Nov 2024; published online 14 Dec 2024. doi: 10.18287/JBPE24.10.040315.

## 1 Introduction

The extensive development of laser medicine, both therapy and diagnosis, is accompanied by the search of methods and instruments for the delivering of light to tissues, which should be characterized by high efficiency and ease of use [1–6]. The instruments, based on fiber optics, have become widespread in clinics, since they allow for compact design, low losses of light propagation and the ability to access hard-to-reach tissues. Different fiber-based probes are applied for intravascular evaluation of plaques, angioplasty, lithotripsy, endoscopy, optical coherence tomography, intraoperative fluorescence diagnosis and other clinical purposes [7–11]. Among them, laser photodynamic and thermal therapy [4, 12–14] also need fiber-based light delivering instruments, which should enable predictable and reproducible exposure, mechanical and chemical stability, as well as to have a compact size. Such instruments can provide either diffused or localized light beams [15–17] and be made of single quartz fiber or special needles/sheaths combined with fibers. Their design varies significantly depending on the required radiation patterns and output beam shape applied for non-contact, contact and interstitial laser surgery and therapy. Localized irradiation is achieved by using conical distal end of a fiber with a small angle of sharpening; other devices include spheres, micro-lenses, domes, faceted shapes, gradient index lenses and tapered fibers [18–21]. The diffused beam is obtained by partial destruction of the fiber cladding, its structuring, application of diffusing sheaths, etc. [13, 14, 22–25].

Routine use of protective sheathes is due to (1) the rapid degradation of quartz during tissue ablation and coagulation, when bare fiber is in contact with tissue, and (2) the fragility of fiber tip, applied for interstitial therapy. Additional liquid or gas cooling helps to avoid carbonization of tissue, which limits further light propagation, and prevents adhering of the instrument to tissue [26–28]. Thus, with the use of increased radiation power, cooled instruments yields higher coagulation volume. Moreover, such probes, either cooled or uncooled, may provide diagnostic puncture or imaging of tissue.

It is quite attractive to assist the laser therapy and ablation with sapphire capillaries for fiber placement. Sapphire has a complex of unique properties that guarantees the absence of any degradation of the optical and mechanical properties under hard physical exposure and in chemically non-neutral environments [29−37]. Besides, it possesses high transparency in visible and near infrared ranges, which makes it suitable for light delivering and implementation of various optical diagnostic and exposure techniques. The application of sapphire for medical purposes was considered previously and has demonstrated high prospective for manufacturing of scalpels, cryosurgical and aspiration probes, along with the capillary needles for laser therapy and ablation [38−44]. Such instruments are characterized by complex shape, which can be achieved by the use of shaped crystal growth techniques [45−50]. Moreover, Stepanov/ Edge-defined Film-fed Growth (EFG) technique is the only method applicable for the manufacturing of sapphire elements with long internal channels with the diameter of 0.5−0.8 mm for fiber accommodation. These channels possess high quality of as-grown surfaces. Additionally, the closed end of the channel protects the inserted fiber from direct contact with tissues during exposure.

The closed-channel design of sapphire crystals applied for medical instruments mainly determines the radiation pattern formed by the instrument in the tissue or on its surface. The external shape of the crystal plays a significant role. Previously, it was demonstrated that a different geometry of the sapphire capillary's tip, formed either by a growing process or by additional mechanical shaping, enables changing the outer beam shape [51, 52]. In particular, it is possible to obtain sub-millimeter focusing of the radiation beam in contact with water medium using micro-focusing sapphire capillary needle [52]. However, the shape of channel bottom formed completely during the process of crystal growth also affects the radiation pattern due to its significant negative curvature.

In this paper, the impact of the channel's form on the radiation pattern is studied in details. We consider the case of a thin capillary needle for surface and interstitial laser ablation combined with quartz fiber with routine numerical aperture. Both numerically and experimentally, we observe the light propagation in tissue caused by this kind of needle with different shapes of the channel bottom. The results show the possibility of forming diffusing light beams as well as narrow collimated beams in the axial direction by choosing particular combinations of the channel's curvature and the tip's angle. Moreover, we have demonstrated the capability for forming the ring pattern with a sharp axial peak without additional diaphragms or spatial light modulators. Our findings are important for further design of sapphire capillary medical instruments and allow for effective application of the sapphire capillary needles for laser therapy and ablation.

## 2 Materials and Methods

### *2.1 Fabrication of Sapphire Needles*

Sapphire capillary needles were produced by the EFG technique [33, 53−58], which relates to methods of growing shaped crystals from a melt. Sapphire needle has the form of a thin tube with monolithic end. The internal channel is completely formed during the growth process, while the end of such crystal can be additionally processed by grinding and polishing to obtain conical shape. The channel is then used for placing optical fiber connected to the light source [34, 52].

The schematic of the growing process is shown in Fig. 1A. The setup includes a growing chamber with a high purity atmosphere of argon. Temperature gradient in crystallization zone was insured by a 22-kHz induction heated graphite susceptor. A crystal shape is determined by the design of a die immersed in the $Al_2O_3$-melt with a temperature of over 2053 °C. Due to the capillary force, the melt rises up through the ring gap with 0.1 mm thickness inside the die. On the top, the melt forms a meniscus, locked by the edges of the die. Thus, the lateral dimensions of a crystal could only vary within a narrow range determined by the volume of the melt meniscus [54, 55]. A sapphire crystal of relatively small cross-section (with outer diameter of ∼1–3 mm) grows with the pulling rate 50−150 mm/h.

The pressure inside of the melt meniscus and its height depends on growth conditions in the crystallization zone. Their changes, both abrupt and continuous, together with the specific design of the die result in the crystal's shape transition. In particular, an increase of temperature and/or pulling rate, a break and reverse of pulling, may cause closing of the channel inside the capillary needle (Fig. 1B), while its opening occurs due to the overcooling in melt meniscus, which leads to the pull-off of melt excesses and melt hooking on internal edge of the die (Fig. 1C). Thus, the actual shape of the channel's bottom depends on the combination of technological conditions and their alteration within a short time period along with the particular shape of the die.

To study the possible channel shapes, we manufactured several capillary needles with the same external and internal diameters, i.e. 1.2 and 0.5 mm, respectively. The representative images of the needle and its cross section are shown in Fig. 1D and E. The bottom of the channel has a regular geometry of an axially symmetrical body, whose form may vary from a near-to-flat surface to approximately spherical and even ellipsoidal one. For our further considerations, we choose several cases (see Fig. 1F) between the maximum and minimum possible curvatures, namely – flat bottom, spherical surfaces with the radiuses $r = 1.25, 0.5, 0.25$ mm and ellipsoidal surface with semi-axes $a_{\mathrm{el}} = 0.25$ and $b_{\mathrm{el}} = 0.5$ mm. We should note that we leave for our future studies the detailed analysis of the technical aspects and their impact on the channel shape.

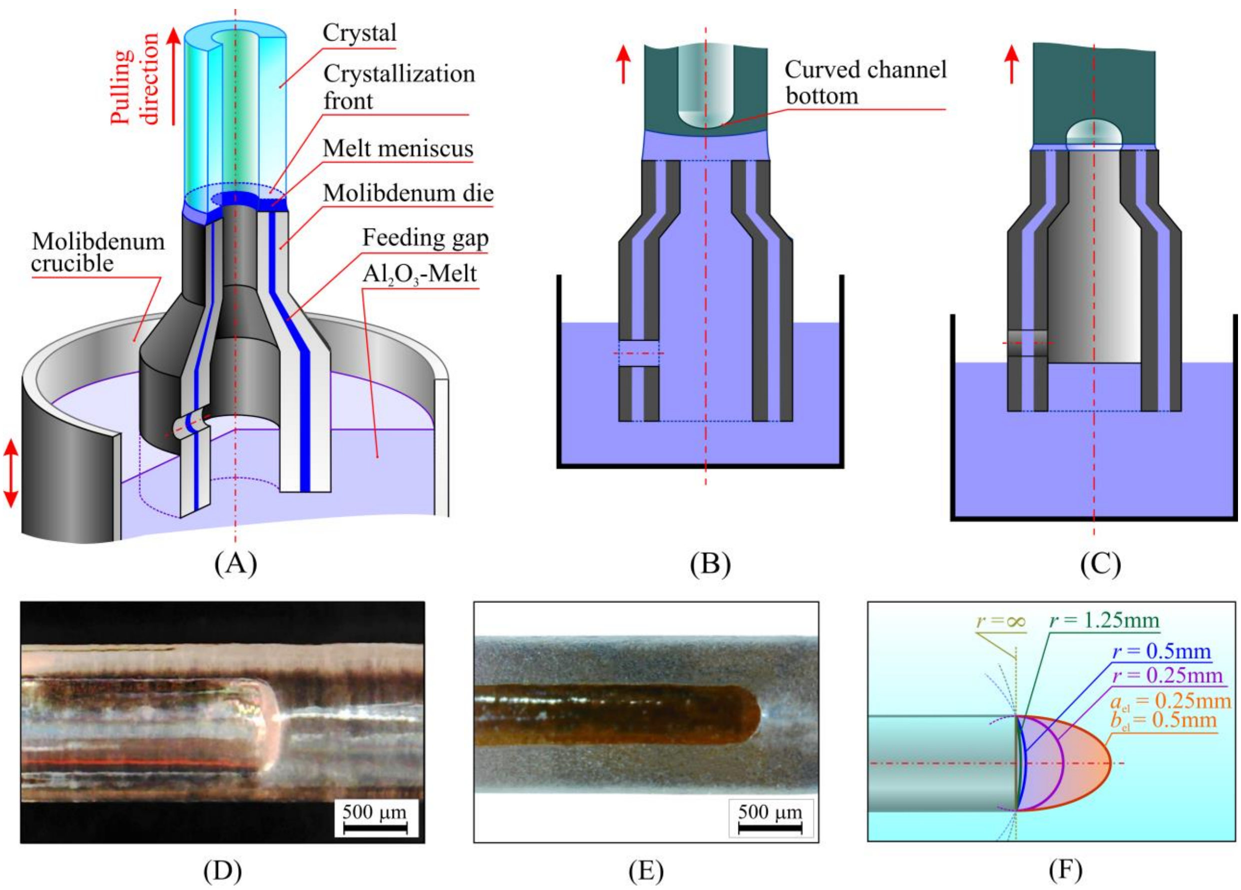


Fig. 1 (A) A schematic of EFG growth of a sapphire capillary needle; (B) "capillary to rod" transition; (C) "rod to capillary" transition; (D) image of a needle with closed channel; (E) the needle's cross section; diameters of the needle and the channel are 1.2 mm and 0.5 mm, respectively; (F) the curvature of channel bottom considered in this work; $r$ stands for the radius of the related sphere, $a_{\mathrm{el}}$ and $b_{\mathrm{el}}$ stand for semi-axes of the related ellipsoid.

In this work, we only observe different curvature of the channel bottom and use it in numerical simulations of radiation patterns to investigate its impact on the output beam shapes.

## *2.2 Numerical Simulations of Radiation Patterns*

The radiation patterns formed at the output end of the sapphire needles were studied numerically by means of the ray tracing approach. Namely, we use the TracePro package for the 3D numerical simulation of photons' migration. We assume that the approximations of geometrical optics are relevant, since the analysis of light–needle interaction is implemented at the scales much larger than the wavelength. In this study, the radiation wavelength $\lambda$ is set to 1.06 µm, which corresponds to one of the most applicable laser sources for tissue coagulation; therefore, the refractive index $n_{\mathrm{s}}$ and the absorption coefficient (by power) $\mu_{\mathrm{a,s}}$ of sapphire are considered to be 1.76 (for ordinary ray) and $10^{-6}$ mm$^{-1}$, respectively. The cylindrical part of the needle has the outer diameter $d_n = 1.2$ mm, while its conical part is characterized by the angle of sharpening $2\gamma$, which varies in the performed numerical simulations. The channel has the diameter $d_c = 0.5$ mm and the position $l_{\mathrm{c}}$ inside the needle (see Fig. 2). It is filled with air ($n = 1$). The curvature of its closed end corresponds to the above-mentioned values $r$, $a_{\mathrm{el}}$ and $b_{\mathrm{el}}$. In this work, multimode optical fiber with the diameter $d_{\mathrm{f}} = 200$ µm, refractive index $n_{\mathrm{f}} = 1.54$ and $\mu_{\mathrm{a,f}} = 3 \cdot 10^{-6}$ mm$^{-1}$ is considered; parameters $z_{\mathrm{f}}$ and $2\omega$ denote its position inside the channel and the numerical aperture (NA), respectively. The output beams have the Gaussian shape. The radiation patterns are analyzed either in free space or in water medium featuring $n_0 = 1.33$ and $\mu_{\mathrm{a,m}} = 0.015$ mm$^{-1}$, in the plane removed from the needle at a distance $L_{\mathrm{an\ pl}}$. The quantitative evaluation of the laser beams in this plane is performed by means of the reduced axial energy $I_{\max}$ and full width at half maximum (FWHM) for Gaussian spatial profile, as it is illustrated in Fig. 2. The grid of rays that set Gaussian spatial profile is represented by a spatial weighting, where each ray has uniform flux and weighted position.

## *2.3 Tissue Samples*

To study the coagulation regions in living tissues performed by the sapphire needles with a specific combination of the needle's tip and the shape of its channel, we have used the *ex vivo* samples of turkey liver.

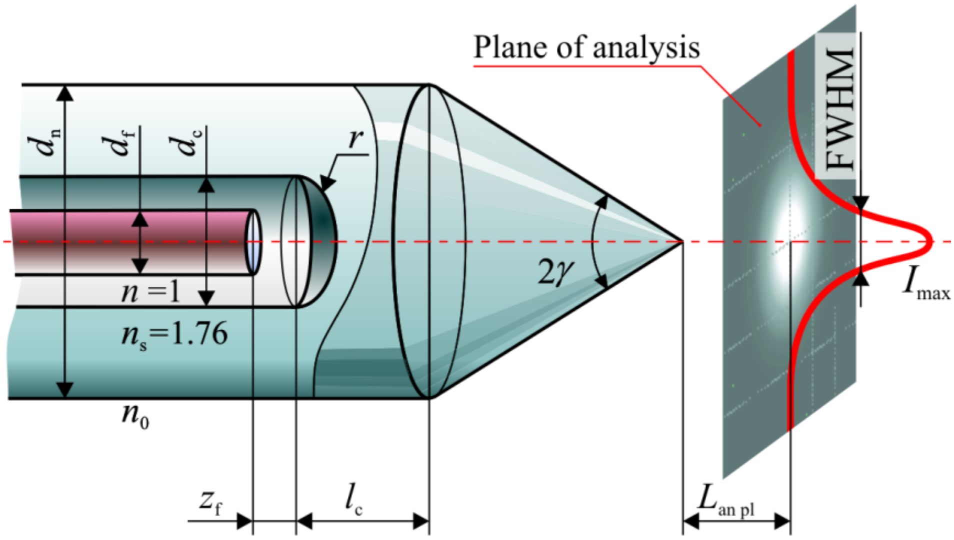


Fig. 2 The scheme of a needle and the parameters used in the numerical simulations.

Such type of tissue effectively absorbs laser radiation of the near infrared range. Before the measurements, the tissue samples with lateral dimensions 40 × 40 mm and 15 mm height were placed in a cuvette then the cuvette was filled with distilled water, covering the surface of the samples by 10 mm. The initial temperature of the samples and water was ambient (24 °C). After performing coagulation, the samples were extracted from the cuvette. The sizes of the coagulated regions were analyzed using digital camera and threshold filtering of the tissue images.

## 3 Results

### 3.1 Beam Shape in Case of Flat Needle's Tip

To analyze the output beam shapes formed by the described sapphire needles, we start with the case of the flat needle's tip ($2\gamma = 180°$) in a free space. Fig. 3 demonstrates the changes of $I_{\max}$ and FWHM right at a needle's distal end ($L_{an\ pl} = 0$), when a common quartz fiber with $2\omega = 40°$ is placed inside the needle's channel at $z_f = 0.1$ mm. It is clear that the curved bottom of the channel acts as an additional refractive interface between air and sapphire with rather high refractive index $n_s = 1.76$. It results in the nonlinear decrease of $I_{\max}$ and blurring of FWHM when the curvature of this interface changes from flat, with $r$ tends to infinity, to ellipsoidal shape (graph point corresponded to $r = 0.125$). The equivalent radius $r = 0.125$ is valid for the referred ellipsoidal shape as all the beam's rays fall on the inner surface in the close vicinity of optical axis.

The most common case of the channel's shape obtained by the EFG technique corresponds to $r \cong d_c/2$. Therefore, for the considered geometry of the needle, we should pay special attention to the area near $r = 0.25$ mm. In its vicinity, the change of the beam parameters strongly depends on even small deviation of $r$, which confirms the need to consider the internal shape of the needle for appropriate planning of the tissue exposure.

Fig. 4(A−D) demonstrates the radiation patterns formed by the needle with flat end in the free space. When the bottom of the capillary channel is also flat or features slight curvature (see panels A and B), the light beam is entirely projected on the output surface of the needle and the beam shape has a regular form. The increase of the bottom's curvature leads to blurring of the beam. At the same time, the more curved channels yield the formation of the ring-like shape of the output beam due to the total internal reflection of the extreme rays from the cylindrical surface of the needle (panels C and D). Such beams are characterized by the appearance of high energy density in the axial direction.

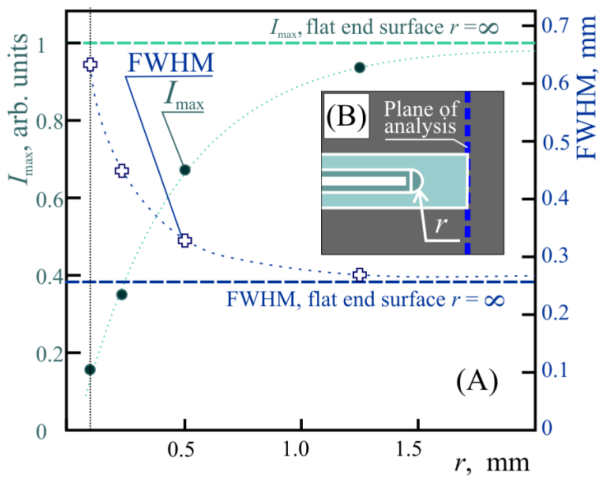


Fig. 3 (A) The change of laser beam parameters (reduced axial energy $I_{\max}$ and FWHM) depending on the curvature $r$ of the channel; numerical simulations performed for a specific needle's form (B) and parameters $l_c = 1$ mm, $z_f = 0.1$ mm, $L_{an\ pl} = 0$ mm, $2\omega = 40°$.

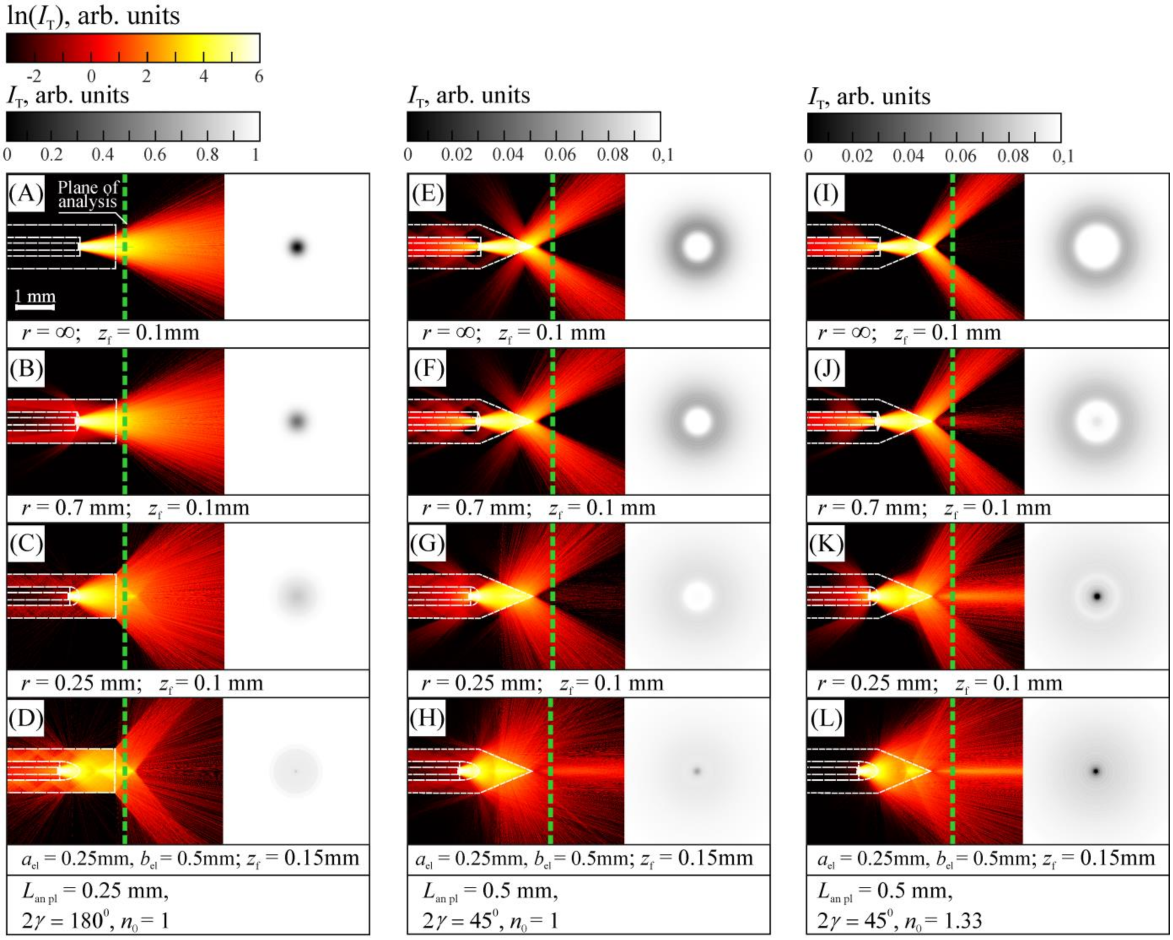


Fig. 4 Numerical simulations of the beam shapes, represented by the transmitted intensity $I_T$, formed by the capillary needles with different curvature of channel's bottom and the quartz fiber with $2\omega = 40°$. (A)−(D) The needle with flat tip is placed in a free space. (E)−(H) The needle with conical tip $2\gamma = 45°$ is placed in a free space. (I)−(L) The needle with conical tip $2\gamma = 45°$ is placed in a water medium.

Despite the flat end of the needle is rarely used for laser therapy, it may be applied for diagnostic sapphire probes [39, 59]. In that case, the channel's curvature may change the diagnostic precision. This fact deserves additional experimental studies, but we leave it for our future work. We account the shape of the needle's conical tip and observe the joint impact of the needle's inner and outer geometry on the beam shape in the following subsections.

### *3.2 Beam Shape in Case of Conical Needle's Tip*

When the needle has conical tip, it can be applied for local high energy concentration of light coming out from the fiber [56, 57]. The multiple total internal reflection of beams in the cone leads to redistribution of energy and the grouping of rays in portions exceeding at different angles to the needle axis. Panels (E−L) in Fig. 4 demonstrate a representative case, when the conical tip has the angle $2\gamma = 45°$. The formation of a ring structure of the output beam shape is clearly observed. Moreover, it depends on the curvature of the channel's bottom. When the latter is flat, the axial part of the output beam is almost absent, and the beam has an obvious annular shape (see panels E and I for distribution of transmitted intensity $I_T$ in a free space and water, respectively). The appearance and further increase of the curvature enlarge the portion of rays unreflected in the cone; thus, it enhances the beam divergence and blurs the rings in the beam shape (see Fig. 5A). Moreover, it leads to the formation of collimated and focused rays transmitted in the outer environment. One can clearly observe the central peak in the beam shapes in panels H and J−L. Obviously, this process is stronger in the medium with a higher refractive index.

The condition for the appearance of the collimated and the focused rays depends on the combination of the aperture angle $2\omega'$ of the ray refracted at the channel's bottom and the tip's angle $2\gamma$ (Fig. 5B). The aperture angle $\omega'$ depends on both the fiber NA and the curvature of the channel. It is clear that for a sharper needle the fiber should have larger NA for the same curvature of the channel. Thus, to obtain an axial beam spot for the focused tissue exposure, the particular combination of the needle and fiber should be chosen.

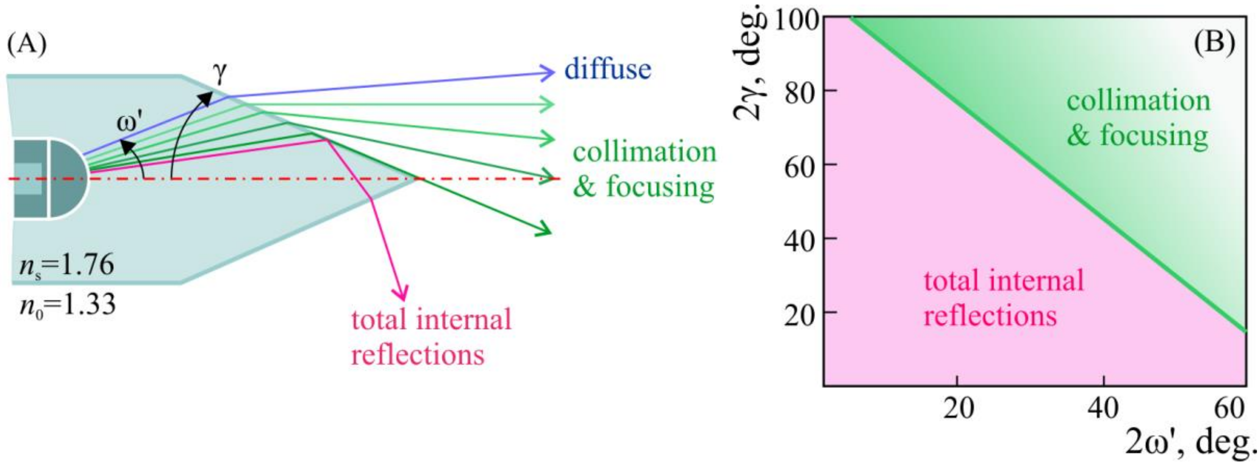


Fig. 5 Appearance of the ring-like, collimated and diffused parts of the beam shape due to different combination of the tip's angle $\gamma$ and the aperture angle $\omega$' of the ray refracted at the channel's bottom. (A) Change of the direction of the output beam due to an increase of $\omega$'. (B) The condition for the appearance of a collimated and focused part of the beam; the needle in water environment is considered. The parameters $l_c = 1$ mm, $z_f = 0.1$ mm are considered.

### 3.2.1 Impact of Different Cone Angle on the Beam Shape

Fig. 6 compares the beam shapes formed by the needles with different cone angles in water medium. While rather sharp tip yields the diffuse beams (A, B) regardless of the shape of the channel bottom, large angle $2\gamma$ leads to beam focusing near the tip end (C, D). However, the ellipsoidal and flat bottoms are rarely expected during the crystal growth. Despite the analysis of beams in such extreme cases is useful, the most common hemispherical channel shape deserves special attention (Fig. 6(E−I)). Near the tip, one can observe the significant impact of the cone angle on the light distribution and, in particular, on the ability of focusing a part of the beam, which is in accordance with Fig. 5B.

Fig. 6J shows the reduced axial energy $I_{\max}$ in the representative case of the needle with $2\gamma = 45°$ and hemispherical bottom of the channel. As it is illustrated in Fig. 6G, such needle forms the collimated and focused part of the output beam. The maximal intensity in the focused part rapidly reduced with the distance $L_{\text{an pl}}$. Moreover, to obtain the highest $I_{\max}$ in the beam spot, one should choose the fibers with $2\omega$ from the range of 24°–34°. The beam parameters for this needle and $2\omega = 34°$ are shown in Fig. 6K. Within the distance $L_{\text{an pl}}$ from 1 to 5 mm, $I_{\max}$ decreases by about 5 times and FWHM of the spot size increases from 80 to 500 μm.

The above analysis is valid for the environments with no scattering or when the needle is slightly removed from the tissue sample. Nevertheless, when the interstitial application is considered, the tissue scattering properties should be accounted. Fig. 7 shows the impact of increased scattering coefficient in the outer environment on the blurring of the focusing beam part. Therefore, a sapphire needle is more likely to form in a tissue a diffuse isotropic-like light distribution concentrated on the needle's end.

### 3.3 Micro-Coagulation of Tissue by Conical Needle

A complex beam shape formed by a sapphire capillary needle gives an opportunity of micro-coagulation of tissues. Since an impact of light scattering in soft tissues is significant, a small distance between the needle's tip and tissue surface should be remained to concentrate most of the beam in a small spot. We have compared experimentally the results of two positions of the needle with angle $2\gamma = 45°$ and hemispherical bottom of the channel (Fig. 8). For this aim, we prepared samples of *ex vivo* liver tissue and placed them in a cuvette filled with water. The water prevents from the dehydration of samples during experiments and also contributes to formation of strong focusing beam part. In the first position, the needle tip touched the sample surface and slightly inserted in it (Fig. 8A). In the second position, the distance between the needle and the sample was 0.5 mm. As it is shown in Fig. 8B, where alignment green beam was used, it allowed us to make a small central spot surrounded by a ring-like beam part. However, the results of numerical simulations demonstrate the blurring of this ring in the tissue volume (Fig. 8D). But the observed localization of beam power inside the tissue in these two cases (C and D) allows us to expect the possibility to perform micro-coagulation.

To study this effect experimentally, the continuous-wave laser source (LAKHTA-MILON, Milon Group, Russia) with the wavelength $\lambda$ =1.06 μm and tunable output power was used. The liver tissues were exposed by this laser for 30 s using uncovered fiber with $d_f = 300$ μm and $NA = 0.14$ and the combination of the fiber with the sapphire needle. Contact and contactless positions were considered as stated above. Panels (E−H) in Fig. 8 demonstrate the representative images of tissue samples after exposure.

 doi: 10.18287/JBPE24.10.040315

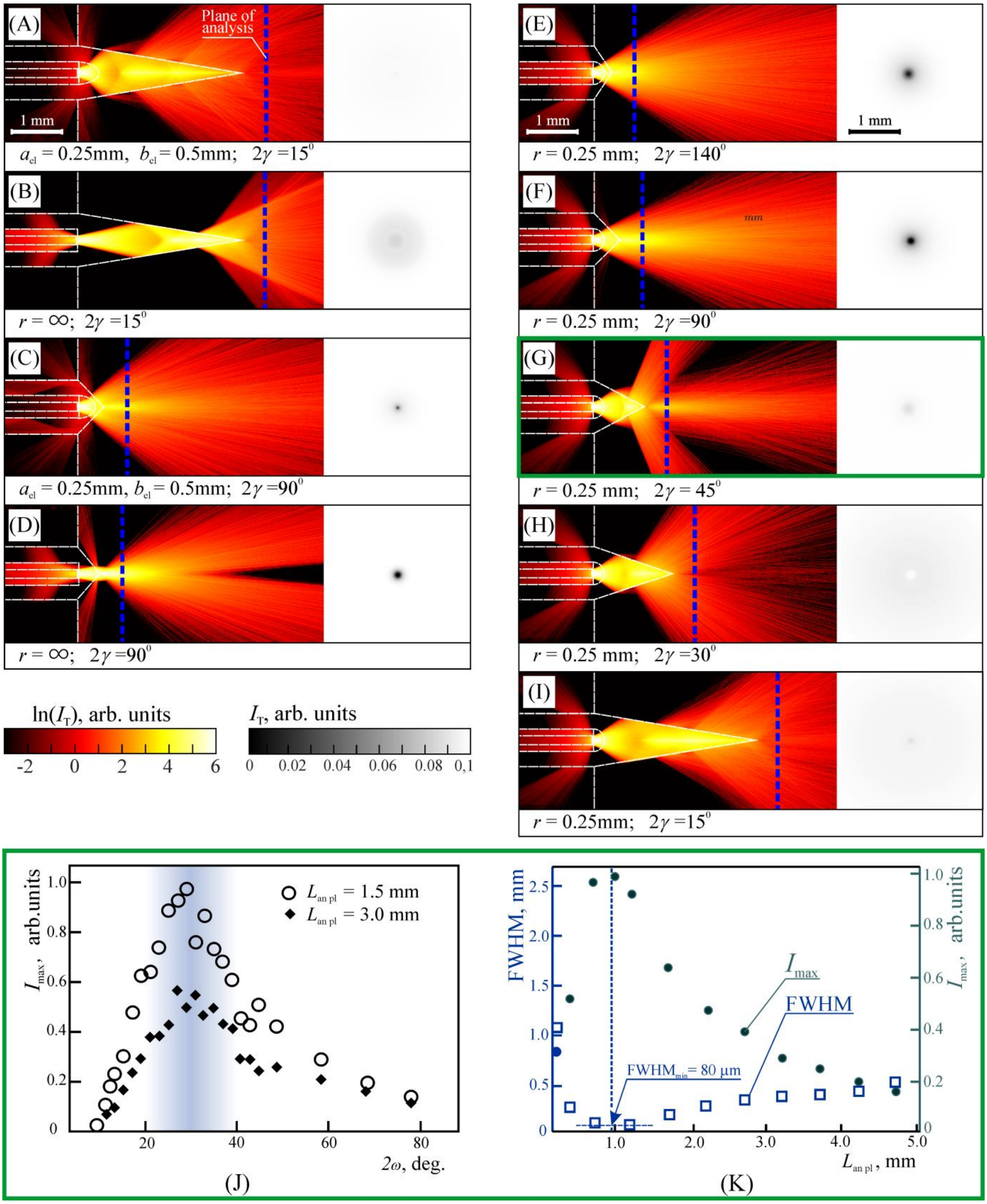


Fig. 6 Numerical simulations of the output beam shapes in water, represented by the transmitted intensity $I_T$, formed by the capillary conical needles and the quartz fiber with $2\omega = 40°$. On the left, the extreme cases of cone angles $2\gamma = 15°$ (A, B) and 90° (C, D) and ellipsoidal (A, C) or flat (B, D) bottom of the channel are shown. (E−I) Beam shapes produced by the needle with hemispherical bottom of the channel and various cone angles. In panels A−I, $L_{an\ pl} = 0.5$ mm, $z_f = 0.1$ mm. (J, K) Output beam parameters in case of $2\gamma = 45°$ and $r = d_c/2 = 0.25$ mm. (J) reduced axial energy $I_{max}$ depending on different fiber NA, (K) beam parameters for $2\omega = 34°$.

 doi: 10.18287/JBPE24.10.040315

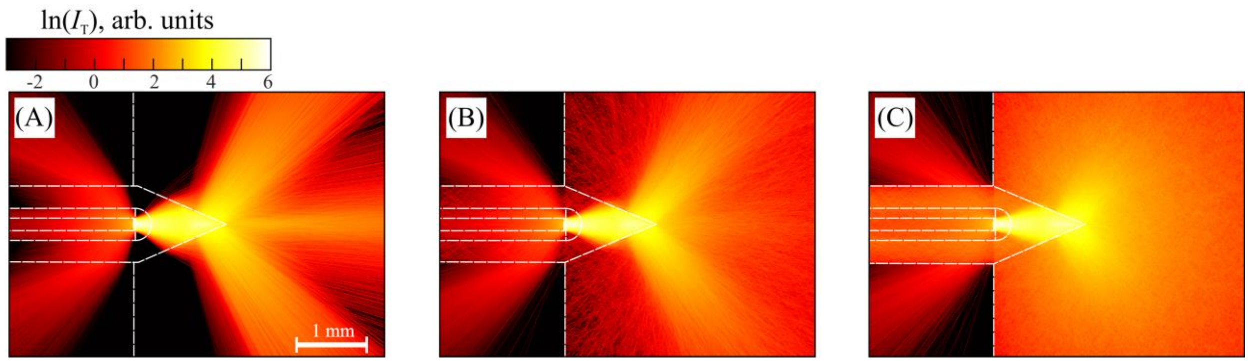


Fig. 7 Numerical simulations of the output beam shapes in the tissue ($n_0$=1.37) with increasing of scattering coefficient μs and decreasing of anisotropy parameter $g$: (A) $g$ = 1, $m_s$ = 1 mm$^{-1}$; (B) $g$ = 0.9, $m_s$ = 1.5 mm$^{-1}$; (C) $g$ = 0.72, $m_s$ = 3.7 mm$^{-1}$; the needle with cone angle $2\gamma = 45°$ and hemispherical channel's bottom is considered, $2\omega$=40°. Absorption is neglected in tissue.

When the uncovered fiber is used, it can lead to the carbonization (panels G and H), which was started at 8 W of laser output power for contactless position and 3 W, when the fiber is in contact with tissue. In contrast, the application of the sapphire needle prevents from tissue carbonization in the observed range of laser power, up to 10 W (panels E and F). But unlike the commonly used diffusers, which are also applied for the same purpose, the coagulation spot remains very narrow and does not exceed 1.5 mm for contactless position. In Fig. 8I, one can compare the diameters of coagulation area. It is clear that choosing the position of the sapphire needle, a rather wide range of coagulation spots from 0.8 up to 3 mm can be achieved without carbonization, including extremely small ones less than 1 mm.

## 4 Discussion

Sapphire capillary needles are unique instruments for surface and interstitial laser therapy. They can be combined with a wide range of light sources and fibers. Despite their small external dimensions of less than 2 mm in diameter, it is possible to manufacture such needles with different shape of their tips. In addition, the capillary channel inside the needle, which is made during the crystal growth process, may possess different bottom curvature. Therefore, the radiation patterns formed by the needles are rather different. Since sapphire has a higher refractive index than quartz, small changes of the needle's shape alter the output beam distribution more noticeably. The condition for total internal reflection inside the conical tip is satisfied for a larger number of rays. The results of this study demonstrate that for these reasons, it is possible to observe diffusing, collimated, focusing or ring-like beams formed by the sapphire needles.

While the diffusing beams are rather common in laser therapy and there are several solutions and instruments for their formation, the focusing needles are of particular interest. As we have shown, in the case of sapphire needles, partial focusing of the output beam can be achieved for a simple conical geometry of the tip, when the angle $\gamma$ is chosen appropriately. In aqueous environment, this effect is more pronounced.

It permits using these needles for local exposure of small tissue area, for example, for coagulation of small metastasis and cysts [16, 60−65]. The point concentration of light near the needle's tip in aqueous solutions can be useful for optogenetics [66, 67], when local stimulation of cells and tissue areas is caused by optical radiation [8, 9]. Application of various gels, including cooling ones, in combination with needle-assisted laser therapy can reduce the localization of tissue destruction even more, when it is important to prevent damage and overheating of surrounding intact tissues. The same effect of local therapy can be achieved in low scattering tissues or hollow organs filled with saline solution.

The principal difference between glass tips, quartz fibers and sapphire needles is the significantly higher thermal conductivity of the latters, which is probably the main reason for the absence of tissue carbonization for contact mode. While coagulation of very small volumes in tissues using uncovered fiber requires exposure of laser power density at much more reduced level in comparison with the combination of the fiber with the sapphire needle, there is still a risk of spontaneous rapid accumulated overheating of fiber. The small changes in thermal conducing properties of irradiator or tissue can cause carbonization hindering the planned growth of coagulated volume. It should be mentioned that carbonization prevents from light penetration in deeper tissues; therefore, laser exposure becomes uneven and unpredictable. Additionally, it can cause damage to glass instruments or unprotected quartz fibers. The sapphire needle removes heat from the tissue more efficiently.

It is essential that the shape of the internal capillary channel plays the same important role as the tip's geometry for the formation of the complex output radiation pattern. The curvature of the channel's bottom should be taken into account, as shown by the demonstrated numerical results. In general, it increases the beam divergence before transmitting the needle's tip, and the output beam includes ring-like diffused radiation and collimated and focused rays.

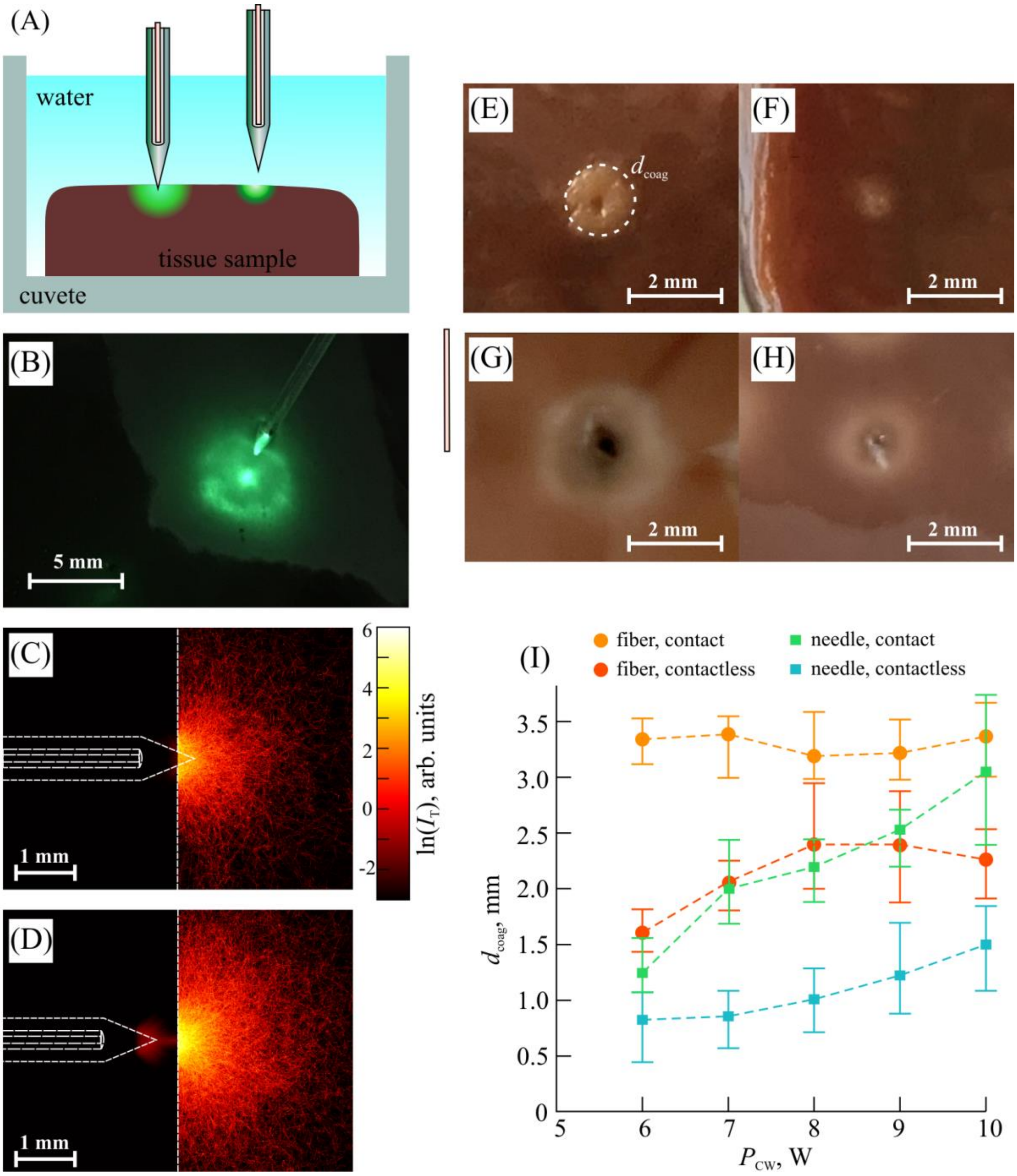


Fig. 8. Experimental study of tissue coagulation by the conical sapphire needle and continuous-wave laser source at 1.06 µm. (A) Positions of the needle during exposure. (B) The beam shape formed contactlessly by the conical needle. (C), (D) The results of numerical simulation of light transport in tissue with parameters $n_0 = 1.37$, $\mu_a = 4.0$ cm$^{-1}$, $\mu_s = 52.13$ cm$^{-1}$, $g = 0.77$, by the needle in two considered positions. (E−H) The representative examples of coagulation of liver tissue by 8 W output power during 30 s, performed by a combination of conical needle with quartz fiber in contact with tissue (E) and remoted from the tissue surface at 0.5 mm (F); (G), (H) – the same for the single fiber. (I) The diameters of coagulation spot $d_{coag}$ obtained in the considered cases during 30 s of exposure; errorbars denote $\pm\sigma$ for the set of 5 measurements.

Since the bottom is produced during the crystal growth process, no additional resources are needed for shaping its curvature. Although the hemispherical shape is the most common, small deviations of the curvature can appear due to alterations of the technological growth parameters. As we have shown in the numerical simulations, the increase of the curvature results in the illumination of the larger tip's surface and in a larger coagulation region in the tissue. Therefore, it is important to estimate the channel shape before applying the needle for laser thermal therapy.

The demonstrated impact of the channel form on the beam shape is of high importance for other types of sapphire crystals with internal capillary channels, manufactured by the EFG technique, such as diagnostic probes and scalpels. For these instruments, the aperture of the output and the detected light beams is one of the key factors for estimating their sensitivity and precision. In this regard, the channel curvature should be considered during the theoretical description of the analyzed optical response from tissues and further signal processing.

Finally, we should mention the capability of growing rather long sapphire needles up to tens of centimeters along with short compact tips. While the former can be used solely for surface or interstitial laser therapy, small cut-off tips can be integrated with endoscopes and other surgical instruments, granting the possibility to use flexible medical tools.

## 5 Conclusion

In this work, the formation of different beam shapes by applying conical sapphire capillary needles for laser thermal therapy was studied numerically and experimentally. The main focus was on the capillary channel inside the needles, grown by the EFG technique. We have analyzed the possible range of the curvature that can be produced in the channel's bottom during the crystal growth process. It was observed that even slight alteration of the curvature dramatically changes the output beam divergence and radiation pattern. Completely different radiation patterns can be obtained by changing the combination of the channel's curvature and the conical angle of the tip. In particular cases of the needle's geometry, the beam can possess strong collimated and focused components as well as a ring-like structure. It can be used effectively for localized coagulation of tissues. To analyze this feasibility more precisely, we have performed coagulation of *ex vivo* liver tissue with such a sapphire needle and a continuous-wave laser source (with 1.06 μm wavelength), comparing the results with the application of a single quartz fiber without a needle or other protection. We have covered the tissue samples with a layer of water for making the beam shape more pronounced. The absence of tissue carbonization along with the precise coagulation was observed for the laser power up to 10 W and application of the sapphire needle, in contrast to using single fiber. Moreover, the sapphire needle allows one to smoothly adjust the coagulation spot from 0.8 up to 3 mm by tuning the laser source power, while the carbonization of tissues appeared for a single fiber prevents this opportunity.

The results of this work revealed the need for accounting the channel shape inside the sapphire capillary needles and posed the question for further research on the crystal growth technological parameters, which have the strongest influence on the final channel's geometry.

## Acknowledgments

This work was supported by the Russian Science Foundation, Project # 24-29-00424.

## Disclosures

The authors declare no conflicts of interest.

## References

1. M. Niemz, Laser-Tissue Interactions: Fundamentals and Applications, 4th ed., Springer, Switzerland (2019). ISBN: 9783030119164.
2. M. R. Hamblin, Y. Huang, Handbook of photomedicine, 1st ed., CRC Press, Boca Raton, FL (2013). ISBN: 9781439884706.
3. A. J. Welch, M. J. C. van Gemert (Eds.), Optical-thermal response of laser-irradiated tissue, 2nd ed., Springer Dordrecht (2011). e-ISBN: 978-90-481-8831-4.
4. G. Shafirstein, D. Bellnier, E. Oakley, S. Hamilton, M. Potasek, K. Beeson, and E. Parilov, "Interstitial photodynamic therapy—a focused review," Cancers 9(2), 12 (2017).
5. T. Vo-Dinh, Biomedical photonics handbook: therapeutics and advanced biophotonics, 2nd ed., CRC Press, Florida (2014).
6. C. M. Pacella, T. Jiang, and G. Mauri, Image-guided laser ablation, Springer, Switzerland (2020). ISBN: 9783030217471.
7. G. Keiser, F. Xiong, Y. Cui, and P. P. Shum, "Review of diverse optical fibers used in biomedical research and clinical practice," Journal of Biomedical Optics 19(8), 080902 (2014).
8. A. Tsakas, C. Tselios, D. Ampeliotis, C. Politi, and D. Alexandropoulos, "Review of optical fiber technologies for optogenetics," Results in Optics 5, 100168 (2021).
9. J. Zou, W. Li, N. Meng, J. Jiang, C. Wu, T. C. Lei, R. Sroka, and Z. Huang, "Evaluation of lensed fibers used in photodynamic therapy (PDT)," Photodiagnosis and Photodynamic Therapy 31, 101924 (2020).
10. N. Katta, A. D. Estrada, A. B. McErloy, and T. E. Milner, "Fiber-laser platform for precision brain surgery," Biomedical Optics Express 13(4), 1985–1994 (2022).
11. T. Stokbroekx, A. De Boer, R. M. Verdaasdonk, M. E. Vuylsteke, and S. R. Mordon, "Commonly used fiber tips in endovenous laser ablation (EVLA): an analysis of technical differences," Lasers in Medical Science 29(2), 501–507 (2014).
12. R. Stafford, D. Fuentes, A. Elliott, J. Weinberg, and K. Ahrar, "Laser-induced thermal therapy for tumor ablation," Critical Reviews in Biomedical Engineering 38(1), 79–100 (2010).

13. T. Vogl, R. Straub, K. Eichler, D. Woitaschek, and M. Mack, "Malignant liver tumors treated with MR imaging-guided laser-induced thermotherapy: experience with complications in 899 patients (2,520 lesions)," Radiology 225(2), 367–377 (2002).
14. A. Carpentier, R. McNichols, R. Stafford, J. Guichard, D. Reizine, S. Delaloge, E. Vicaut, D. Payen, A. Gowda, and B. George, "Laser thermal therapy: Real-time MRI-guided and computer-controlled procedures for metastatic brain tumors," Lasers in Surgery and Medicine 43(10), 943–950 (2011).
15. C. Pantaleone, S. Dymling, and J. Axelsson, "Optical fiber solutions for laser ablation of tissue and immunostimulating interstitial laser thermotherapy – Product development in the network of developers, industry and users," Photonics and Lasers in Medicine 5(1), 69–75 (2016).
16. U. Salem, V. A. Kumar, J. E. Madewell, D. F. Schomer, D. C. De Almeida Bastos, P. O. Zinn, J. S. Weinberg, G. Rao, S. S. Prabhu, and R. R. Colen, "Neurosurgical applications of MRI guided laser interstitial thermal therapy (LITT)," Cancer Imaging 19(65), 1–13 (2019).
17. J. Li, C. Shang, Y. Rong, J. Sun, Y. Cheng, B. He, Z. Wang, M. Li, J. Ma, B. Fu, and X. Ji, "Review on laser technology in intravascular imaging and treatment," Aging and Disease 2, 13(1), 246–266 (2022).
18. R. Verdaasdonk, C. Borst, "Ray tracing of optically modified fiber tips. 1: spherical probes," Applied Optics 30(16), 2159–2171 (1991).
19. K. Iwai, Y.-W. Shi, M. Endo, K. Ito, Y. Matsuura, M. Miyagi, and H. Jelinkova, "Penetration of high-intensity Er:YAG laser light emitted by IR hollow optical fibers with sealing caps in water," Applied Optics 43(12), 2568–
20. T. Watanabe, Y. Matsuura, "Side-firing sealing caps for hollow optical fibers," Lasers in Surgery and Medicine 38(8), 792–797 (2006).
21. T. Hutchens, A. Darafsheh, A. Fardad, A. Antoszyk, H. Ying, V.Astratov, and N. Fried, "Novel microsphere chain fiber tips for use in mid-infrared ophthalmic laser surgery," Optical Fibers and Sensors for Medical Diagnostics and Treatment Applications XII, 8218, 18–25 (2012).
22. L. Vesselov, W. Whittington, and L. Lilge, "Design and performance of thin cylindrical diffusers created in Ge-doped multimode optical fibers," Applied Optics 44(14), 2754–2758 (2005).
23. A. Roggan, "Laser applicators for interstitial coagulation," in Applied Laser Medicine, H.-P. Berlien, G. Müller (Eds.), Springer-Verlag, Berlin, Heidelberg and New York, 165–167 (2003).
24. V. Knappe, A. Roggan, M. Glotz, M. Müller, J.-P. Ritz, C.-T. Germer, and G. Müller, "New flexible applicatorsfor laser-induced thermotherapy," Medical Laser Application 16(2), 73–80 (2001).
25. J. C. Mizeret, H. E. Van Den Bergh, "Cylindrical fiberoptic light diffuser for medical applications," Lasers in Surgery and Medicine 19(2), 159–167 (1996).
26. B. Anvari, M. Motamedi, J. H. Torres, S. Rastegar, and E. Orihuela, "Effects of surface irrigation on the thermal response of tissue during laser irradiation," Lasers in Surgery and Medicine 14(4), 386–395 (1994).
27. B. Anvari, B. S. Tanenbaum, W. Hoffman, S. Said, T. E. Milner, L.-H. L. Liaw, and J. S. Nelson, "Nd:YAG laser irradiation in conjunction with cryogen spray cooling induces deep and spatially selective photocoagulation in animal models," Physics in Medicine & Biology 42(2), 265–282 (1997).
28. W. Whelan, D. Wyman, "Dynamic modeling of interstitial laser photocoagulation: implications for lesion formation in liver *in vivo*," Lasers in Surgery and Medicine 24, 202–208 (1999).
29. R. M. Verdaasdonk, C. F. P. van Swol, "Laser light delivery systems for medical applications," Physics in Medicine & Biology 42(5), 869‒894 (1997).
30. P. Möller, L. Lindberg, P. Henriksson, B. Persson, and K. Tranberg, "Interstitial laser thermotherapy: Comparison between bare fibre and sapphire probe," Lasers in Medical Science 10(3), 193–200 (1995).
31. T. Eguro, A. Aoki, T. Maeda, A. A. Takasaki, M. Hasegawa, M. Ogawa, T. Suzuki, K. Yonemoto, I. Ishikawa, Y. Izumi, and I. Katsuumi, "Energy output reduction and surface alteration of quartz and sapphire tips following Er:YAG laser contact irradiation for tooth enamel ablation," Lasers in Surgery and Medicine 41(8), 595–604 (2009).
32. V. N. Kurlov, S. N. Rossolenko, N. V. Abrosimov, and K. Lebbou, "Shaped Crystal Growth," Chapter 5 in Crystal Growth Processes Based on Capillarity Czochralski, Floating Zone, Shaping and Crucible Techniques, Th. Duffar (Eds.), John Wiley & Sons, 277‒354 (2010).
33. G. M. Katyba, K. I. Zaytsev, I. N. Dolganova, I. A. Shikunova, N. V. Chernomyrdin, S. O. Yurchenko, G. A. Komandin, I. V. Reshetov, V. V. Nesvizhevsky, and V. N. Kurlov, "Sapphire shaped crystals for waveguiding, sensing and exposure applications," Progress in Crystal Growth and Characterization of Materials 64(4), 133–151 (2018).
34. I. Dolganova, I. Shikunova, G. Katyba, A. Zotov, E. Mukhina, M. Shchedrina, V. Tuchin, K. Zaytsev, and V. Kurlov, "Optimization of sapphire capillary needles for interstitial and percutaneous laser medicine," Journal of Biomedical Optics 24(12), 1–7 (2019).
35. V. Kurlov, I. Shikunova, A. Ryabova, and V. Loschenov, "Sapphire smart scalpel," Bulletin of the Russian Academy of Sciences Physics 73(10), 1420–1423 (2009).
36. I. Shikunova, V. Volkov, V. Kurlov, and V. Loschenov, "Sapphire needle capillaries for laser medicine," Bulletin of the Russian Academy of Sciences Physics 73(10), 1345–1348 (2009).

37. I. Shikunova, D. Stryukov, S. Rossolenko, A. Kiselev, and V. Kurlov "Neurosurgery contact handheld probe based on sapphire shaped crystal," Journal of Crystal Growth 457, 265–269 (2017).
38. I. N. Dolganova, D. A. Varvina, I. A. Shikunova, A. I. Alekseeva, P. A. Karalkin, M. R. Kuznetsov, P. V. Nikitin, A. K. Zotov, E. E. Mukhina, G. M. Katyba, K. I. Zaytsev, V. V. Tuchin, and V. N. Kurlov, "Proof of concept for the sapphire scalpel combining tissue dissection and optical diagnosis," Lasers in Surgery and Medicine 54(4), 611–622 (2021).
39. I. Shikunova, I. Dolganova, G. Katyba, K. Zaitsev, and V. Kurlov, "Sapphire neurosurgical probe for aspiration of brain tumors with boundary demarcation by use of spectroscopy," Optics and Spectroscopy 126(5), 545–553 (2019).
40. I. Shikunova, I. Dolganova, A. Kuznetsov, E. Mukhina, L. Safonova, K. Zaytsev, and V. Kurlov, "Sapphire crystal cryoapplicators enabling control of cryosurgery based on light-tissue interaction," Cryobiology 92, 278 (2020).
41. I. N. Dolganova, A. K. Zotov, S. N. Rossolenko, I. A. Shikunova, S. L. Shikunov, K. B. Dolganov, K. I. Zaytsev, and V. N. Kurlov, "Manufacturing of hollow sapphire crystal with variable shapes for cryosurgical applications," Crystals 14(4), 346 (2024).
42. I. N. Dolganova, A. K. Zotov, L. P. Safonova, I. V. Reshetov, K. I. Zaytsev, and V. N. Kurlov, "Feasibility test of a sapphire cryoprobe with optical monitoring of tissue freezing," Journal of Biophotonics 16(3), e202200288 (2023).
43. G. M. Katyba, S. P. Lebedev, A. S. Kucheryavenko, I. N. Dolganova, N. V. Chernomyrdin, M. G. Burdanova, I. E. Spektor, M. Skorobogatiy, V. N. Kurlov, and K. I. Zaytsev, "Terahertz refractometry of hard-to-access objects using the sapphire endoscope suitable for harsh environments," Applied Physics Letters 124(24), 243703 (2024).
44. A. A. Platonova, P. V. Aleksandrova, A. I. Alekseeva, S. P. Kudryavtseva, A. K. Zotov, K. I. Zaytsev, K. B. Dolganov, I. V. Reshetov, V. N. Kurlov, and I. N. Dolganova, "Feasibility of monitoring tissue properties during microcirculation disorder using a compact fiber-based probe with sapphire tip," Journal of Biophotonics 17(11), e202400368 (2024).
45. H. E. LaBelle, "Growth of controlled profile crystals from the melt: Part II - Edge-defined, film-fed growth (EFG)," Materials Research Bulletin 6(7), 581–589 (1971).
46. H. E. LaBelle, "EFG, the invention and application to sapphire growth," Journal of Crystal Growth 50, 8–17 (1980).
47. N. Abrosimov, V. Kurlov, and S. Rossolenko, "Automated control of Czochralski and shaped crystal growth processes using weighing techniques," Progress in Crystal Growth and Characterization of Materials 46(1–2), 1–57 (2003).
48. P. I. Antonov, V. N. Kurlov, "New advances and developments in the Stepanov method for the growth of shaped crystals," Crystallography Reports 47(1), S43–S52 (2002).
49. V. N. Kurlov, "Sapphire: Properties, Growth, and Applications," in: Encyclopedia of Materials: Science and Technology, S. Hashmi (Ed.), Elsevier, 8259–8264 (2001).
50. P. Antonov, V. Kurlov, "A review of developments in shaped crystal growth of sapphire by the Stepanov and related techniques," Progress in Crystal Growth and Characterization of Materials 44(2), 63–122 (2002).
51. I. Dolganova, I. Shikunova, G. Katyba, A. Zotov, E. Mukhina, M. Shchedrina, V. Tuchin, K. Zaytsev, and V. Kurlov, "Optimization of sapphire capillary needles for interstitial and percutaneous laser medicine," Journal of Biomedical Optics 24(12), 128001 (2019).
52. I. Dolganova, A. Zotov, I. Shikunova, K. Zaytsev, P. Aleksandrova, E. Mukhina, and V. Kurlov, "Experimental study of pointed sapphire needles for interstitial laser therapy," Society of Photo-Optical Instrumentation Engineers, 11458, 114580E (2020).
53. I. Dolganova, I. Shikunova, A. Zotov, M. Shchedrina, I. Reshetov, K. Zaytsev, and V. Tuchin, V. Kurlov, "Microfocusing sapphire capillary needle for laser surgery and therapy: Fabrication and characterization," Journal of Biophotonics 13(10), e202000164 (2020).
54. S. Rossolenko, G. Katyba, I. Dolganova, I. Shikunova, D. Stryukov, K. Zaytsev, and V. Kurlov, "Numerical Analysis of Liquid Menisci in the EFG Technique," Chapter 3 in Crystal Growth, V. Glebovsky (Ed.), IntechOpen, London (2019).
55. S. Rossolenko, I. Shikunova, V. Kurlov, and S. Shikunov, "Growth of sapphire ribbons with capillary channels for laser spectroscopy," Inorganic Materials: Applied Research 2, 381–386 (2011).
56. R. M. Verdaasdonk, C. Borst, "Optical characteristics of sapphire laser scalpels analyzed by ray-tracing," Society of Photo-Optical Instrumentation Engineers 1420(6), 136–140 (1991).
57. I. Melnik, N. Denisov, and I. Kravchenko, "Light concentration by modified fiber tips and attached scalpel probes," Society of Photo-Optical Instrumentation Engineers 2328, 58 (1994).
58. I. Carneiro, S. Carvalho, R. Henrique, L. Oliveira, and V. V. Tuchin, "Measuring optical properties of human liver between 400 and 1000 nm," Quantum Electronics 49, 13 (2019).
59. A. K. Zotov, A. V. Pushkarev, A. I. Alekseeva, K. I. Zaytsev, S. S. Ryabikin, D. I. Tsiganov, D. A. Zhidkov, I. A. Burkov, V. N. Kurlov, and I. N. Dolganova, "Optical sensing of tissue freezing depth by sapphire cryo-applicator and steady-state diffuse reflectance analysis," Sensors 24, 3655 (2024).
60. M. Nikfarjam, V. Muralidharan, C. Malcontenti-Wilson, and C. Christophi, "Progressive microvascular injury in liver and colorectal liver metastases following laser induced focal hyperthermia therapy," Lasers in Surgery and Medicine 37, 64–73 (2005).

61. M. Havel, C. Betz, A. Leunig, and R. Sroka, "*Diode laser-induced tissue effects: in vitro tissue model study and in vivo* evaluation of wound healing following non-contact application," Lasers in Surgery and Medicine 46(6), 449–455 (2014).
62. F. Pisanello, G. Mandelbaum, M. Pisanello, I. A. Oldenburg, L. Sileo, J. E. Markowitz, R. E. Peterson, A. Della Patria, T. M. Haynes, M. S. Emara, B. Spagnolo, S. R. Datta, M. De Vittorio, and B. L. Sabatini, "Dynamic illumination of spatially restricted or large brain volumes via a single tapered optical fiber," Nature Neuroscience 20, 1180–1188 (2017).
63. J. Stujenske, T. Spellman, and J. Gordon, "Modeling the spatiotemporal dynamics of light and heat propagation for *in vivo* optogenetics," Cell Reports 12 (3), 525–534 (2015).
64. A. Shalabi, A. Ehab, S. F. Shalabi, G. Kugler, H.-J. Schäfers, and T. Graeter, "Laser assisted pulmonary metastasectomy promises a low local recurrence rate," Nature Neuroscience 14, 5988 (2024).
65. H. Fu, F. Luo, and H. Zhao, "A pilot study of minimal invasion combined PDL/Nd:YAG laser in treating facial epidermoid cyst," Journal of Cosmetic Dermatology 20(3), 2805-2809 (2021).
66. B. Spagnolo, A. Balena, R. T. Peixoto, M. Pisanello, L. Sileo, M. Bianco, A. Rizzo, F. Pisano, A. Qualtieri, D. D. Lofrumento, F. De Nuccio, J. A. Assad, B. L. Sabatini, M. De Vittorio, and F. Pisanello, "Tapered fibertrodes for optoelectrical neural interfacing in small brain volumes with reduced artefacts," Nature Materials 21, 826–835 (2022).
67. V. Emiliani, E. Entcheva, R. Hedrich, P. Hegemann, K. R. Konrad, C. Lüscher, M. Mahn, Z.-H. Pan, R. R. Sims, J. Vierock, and O. Yizhar, "Optogenetics for light control of biological systems," Nature Reviews Methods Primers 2, 55 (2022).